

## Article

# Synthesis and Characteristics of $\text{Sr}_3\text{La}(\text{PO}_4)_3:\text{Eu}^{3+}$ Phosphor with Luminescence in NIR Biological Window

Su-Hua Yang \* and Wei-Jun Wang

Department of Electronic Engineering, National Kaohsiung University of Science and Technology, Taiwan

\* Correspondence: [shya@nkust.edu.tw](mailto:shya@nkust.edu.tw); Tel.: +886-7-3814526

Received: Apr 30, 2021; Accepted: Jun 16, 2021; Published: Jul 31, 2021

**Abstract:** The  $\text{Sr}_3\text{La}(\text{PO}_4)_3:\text{Eu}^{3+}$  (SLP:Eu<sup>3+</sup>) phosphor was prepared with the coprecipitation method, which emitted red visible-light along with a near-infrared (NIR) luminescence in the biological window region. The influence of synthesis temperature and Eu<sup>3+</sup> doping concentration on the characteristics of the phosphor was discussed. The optimal crystallinity was obtained when the phosphor was doped with 0.7 mol% of Eu<sup>3+</sup> and annealed at 1200 °C for 2 h. The particle size was approximately 1 μm. As compared with the SLP:0.01 Eu<sup>3+</sup>, the photoluminescence intensity of the SLP:0.07 Eu<sup>3+</sup> increased by 4.95-fold at wavelength of 615 nm and 3.97-fold at 705 nm. The red SLP:Eu<sup>3+</sup> phosphor with a high NIR emission is a potential candidate material for bio-image and bio-sensor applications.

**Keywords:** Phosphor, Near-infrared luminescence, Biological window, Coprecipitation

## 1. Introduction

Eulytite-type orthophosphates have attracted much attention as the host of phosphors, which have a general molecular formula of  $\text{M}_3\text{M}^{\text{II}}(\text{PO}_4)_3$ . The MI can be alkaline earth metals of Ca, Sr, Ba and Pb, and the MII are La, Y, Sc, Bi, Tb and In.  $\text{Sr}_3\text{La}(\text{PO}_4)_3$  [1],  $\text{Ba}_3\text{Y}(\text{PO}_4)_3$  [2],  $\text{Sr}_3\text{Y}(\text{PO}_4)_3$  [3],  $\text{Sr}_3\text{Gd}(\text{PO}_4)_3$  [4], and  $\text{Ba}_3\text{La}(\text{PO}_4)_3$  [5] belong to the family of eulytite-type orthophosphates. These hosts doped with lanthanide activators usually exhibit excellent thermal stability and optical property.

For the red lanthanide activators, Eu<sup>3+</sup> [6,7], Pr<sup>3+</sup> [8], Sm<sup>3+</sup> [9,10] are the most preferred materials. However, they show diverse luminescence characteristics. For the Pr<sup>3+</sup> activator [11–13], a broad energy absorption band with a peak at wavelength approximately of 270 nm is measured, which is resulted from the inter-configurational transition of  $4f^2 \rightarrow 4f^15d^1$ . The electrons transit from the <sup>3</sup>H<sub>4</sub> ground state to higher 4f levels of <sup>3</sup>P<sub>2</sub>, <sup>1</sup>I<sub>6</sub>, <sup>3</sup>P<sub>1</sub>, <sup>3</sup>P<sub>0</sub>, <sup>1</sup>D<sub>2</sub> are also possible. When the Pr<sup>3+</sup> ions are excited with a wavelength of 270 nm, a high luminescence at wavelength 632 nm caused by electron transition of <sup>1</sup>D<sub>2</sub> → <sup>3</sup>H<sub>4</sub> is analyzed. The emission at wavelength 725 nm for electron transition from <sup>1</sup>D<sub>2</sub> → <sup>3</sup>H<sub>4</sub> is relatively insignificant. For the Sm<sup>3+</sup> activator [14–16], the energy absorption peaks are at wavelengths of 378, 402, 440, 468 and 481 nm, attributed to electron transitions of <sup>6</sup>H<sub>5/2</sub> → <sup>6</sup>P<sub>7/2</sub>, <sup>6</sup>H<sub>5/2</sub> → <sup>4</sup>F<sub>7/2</sub>, <sup>6</sup>H<sub>5/2</sub> → <sup>4</sup>G<sub>9/2</sub>, <sup>6</sup>H<sub>5/2</sub> → <sup>4</sup>I<sub>13/2</sub>, <sup>6</sup>H<sub>5/2</sub> → <sup>4</sup>I<sub>11/2</sub>, respectively. The maximum energy absorption peak is at 402 nm. The red Sm<sup>3+</sup> emission shows the highest intensity at 604 nm according to the <sup>4</sup>G<sub>5/2</sub> → <sup>6</sup>H<sub>7/2</sub> transition. The other emission peaks are at 567, 650, and 709 nm referred to the electron transitions from the <sup>4</sup>G<sub>5/2</sub> to the <sup>6</sup>H<sub>5/2</sub>, <sup>6</sup>H<sub>9/2</sub>, and <sup>6</sup>H<sub>11/2</sub>, respectively.

Both Pr<sup>3+</sup> and Sm<sup>3+</sup> show red emission in the visible-light region, but they exhibit low luminescence intensity in the near-infrared (NIR) region. In contrast, the Eu<sup>3+</sup> activator can not only show a high red luminescence but also exhibit a NIR emission within the biowindow [17]. The phosphors with luminescence in the biowindow have high potential for bio-image and bio-sensor applications [18–22]. In this study, the  $\text{Sr}_3\text{La}(\text{PO}_4)_3$  (SLP) was used as host and the SLP:Eu<sup>3+</sup> was synthesized with the coprecipitation method [23–25]. The characteristics of the red SLP:Eu<sup>3+</sup> phosphor are discussed.

## 2. Materials and Methods

The coprecipitation method was used for the synthesis of the red SLP:Eu<sup>3+</sup> phosphor. The source materials were Sr(NO<sub>3</sub>)<sub>2</sub> (99%, Acros), La(NO<sub>3</sub>)<sub>3</sub>·6H<sub>2</sub>O (99.9%, Alfa Aesar), (NH<sub>4</sub>)<sub>2</sub>HPO<sub>4</sub> (99%, Showa), Eu(NO<sub>3</sub>)<sub>3</sub>·6H<sub>2</sub>O (99.9%, Alfa), and NH<sub>4</sub>OH. First, the materials were weighed by the stoichiometric ratio. The concentration of Eu<sup>3+</sup> was varied from 1 to 9 mol%. The Sr(NO<sub>3</sub>)<sub>2</sub>, La(NO<sub>3</sub>)<sub>3</sub>·6H<sub>2</sub>O, and Eu(NO<sub>3</sub>)<sub>3</sub>·6H<sub>2</sub>O were dissolved in deionized (DI) and stirred to form a blended solution. The (NH<sub>4</sub>)<sub>2</sub>HPO<sub>4</sub> was also dissolved with DI water. These solutions were mixed and used as the precursor solution. After that, the NH<sub>4</sub>OH was dripped

into the precursor solution. The precipitation took place when a pH value of 6 was achieved. Subsequently, the obtained precursor was centrifuged, washed, and dried at 120 °C for 2 h. Finally, the precursor powder was annealed at 1000–1300 °C for 2 h.

The X-ray diffraction (XRD, SIEMENS D5000) and field-emission scanning electron microscopy (FESEM, JEOL JSM-6330 TF) were used for the analysis of the crystallinities and morphologies of the phosphors. A fluorescence spectrophotometer (Hitachi F-7000) was used to measure the energy absorption and emission characteristics of the phosphors. The photoluminescence (PL) and PL excitation (PLE) spectra were analyzed at the excitation wavelength ( $\lambda_{ex}$ ) and monitored wavelength ( $\lambda_{em}$ ) of 394 and 615 nm, respectively.

### 3. Results and Discussion

The characteristics of the red SLP:Eu<sup>3+</sup> phosphor was optimized via the variation of the annealing temperature and the doping concentration of the Eu<sup>3+</sup>. Figure 1 shows the XRD patterns of SLP:Eu<sup>3+</sup> synthesized at 1000–1300 °C. It is observed that when the synthesis temperature was lower than 1000 °C, the SLP phase was not synthesized completely. The SLP phase was obtained when the synthesis temperature was higher than 1100 °C. The XRD pattern of SLP:Eu<sup>3+</sup> was consistent with the standard pattern of JCPDS No. 29-1306 and no miscellaneous phases were developed. The as-prepared SLP:Eu<sup>3+</sup> had a cubic structure, the dominant crystal plane was (310) [26]. The particle size of phosphor was increased from 1 to 2  $\mu\text{m}$  when the synthesis temperature was increased from 1000 to 1300 °C, as shown in Figure 2.

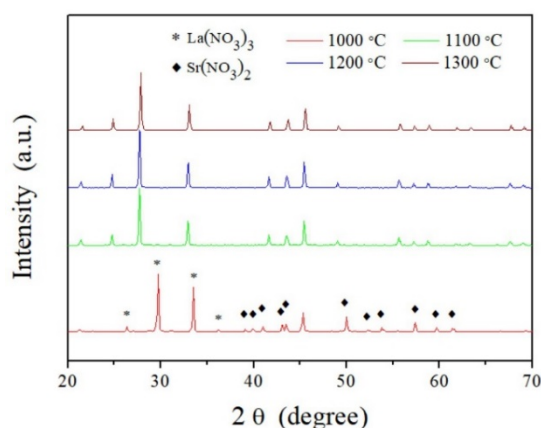


**Figure 1.** XRD patterns of SLP:0.07Eu<sup>3+</sup> synthesized at 1000–1300 °C for 2 h.

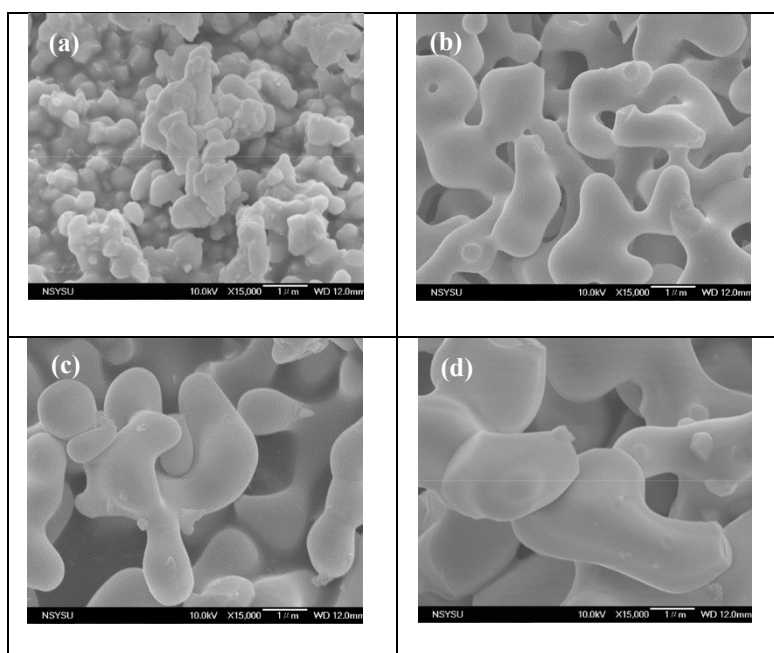


**Figure 2.** SEM images of SLP:0.07Eu<sup>3+</sup> synthesized at 1000–1300 °C for 2 h. (a) 1000 °C; (b) 1100 °C; (c) 1200 °C; (d) 1300 °C.

As it shown in Figure 1 that the crystallization of phosphor was improved with the increase of synthesis temperature. Thus, the synthesis temperature significantly altered with the energy absorption and emission of the phosphor. As compared with the phosphor prepared at 1000 °C, the PLE intensity at wavelength of 394 nm was enhanced by 2.17-, 2.58-, and 2.59-fold and the PL intensity at 615 nm was increased by 1.52-, 1.75-, and 1.80-fold when synthesis temperature was set at 1000 °C, 1100 °C, 1200 °C, and 1300 °C, respectively, as observed from Figure 3. Herein, the 394 nm was the wavelength of the maximum energy absorption peak, attributed to the electron transition of  ${}^7F_0 \rightarrow {}^5L_6$  in  $\text{Eu}^{3+}$ , and the 615 nm was the highest energy emission peak, which was resulted from the electron transition of  ${}^5D_0 \rightarrow {}^7F_2$ . The phosphor prepared at 1200 °C and 1300 °C have the same PL intensity, while a larger particle size was synthesized at 1300 °C.

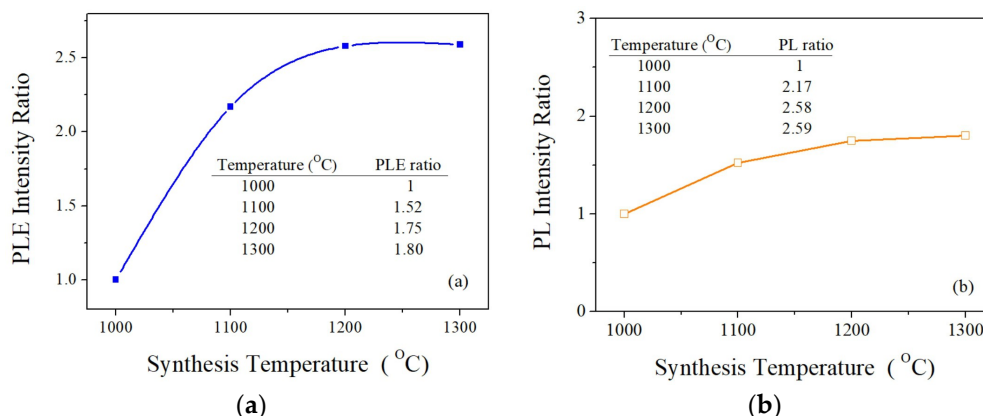


**Figure 3.** (a) PLE and (b) PL intensity ratios of SLP:0.07Eu<sup>3+</sup> synthesized at 1000–1300 °C for 2 h.

When 1–9 mol% of  $\text{Eu}^{3+}$  was doped in the SLP, no new phases were developed. The XRD analysis indicated that the smallest value of full width at half maximum (FWHM) of XRD and the optimal crystallinity of SLP:Eu<sup>3+</sup> was obtained when 7 mol% of  $\text{Eu}^{3+}$  was doped, as listed in Table 1. In the SLP:0.07Eu<sup>3+</sup>, the atomic composition of O, P, Sr, La, and Eu, analyzed using energy dispersive x-ray spectrometer (EDS), were 66.56, 11.38, 15.76, 5.08, and 1.22 at%, respectively, as listed in Table 2. Clearly, the SLP:0.07Eu<sup>3+</sup> with stoichiometric ratio was synthesized. The  $\text{Eu}^{3+}$  was doped into the SLP crystal and formed a solid solution. The elements that exist within the SLP:0.07Eu<sup>3+</sup> were further identified using the x-ray photoelectron spectroscopy (XPS), as shown in Figure 4. The elements of O, P, Sr, La, and Eu were analyzed. For O 1s, which showed a broad peak at binding energy of 530.5–532.5 eV. The La 3d peak was located at 830–837 eV, and the Sr 3d, P 2p, and Eu 4d peaks were at 129–138 eV [26,27].

**Table 1.** FWHM of XRD for phosphor synthesized with different  $\text{Eu}^{3+}$  concentrations.

Eu <sup>3+</sup> Concentration (mol%)	FWHM XRD ( $\Delta 2\theta$ )
1	0.21
3	0.19
5	0.16
7	0.16
9	0.22

**Table 2.** Element composition of SLP:0.07Eu<sup>3+</sup> phosphor synthesized 1200 °C for 2 h.

Element	Atomic Ratio (%)
O	66.56
P	11.38
Sr	15.76
La	5.08
Eu	1.22

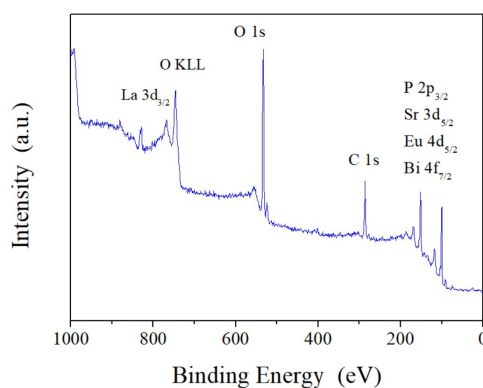


**Figure 4.** XPS spectrum of SLP:0.07Eu<sup>3+</sup> phosphor synthesized 1200 °C for 2 h.

The energy absorption and luminescence of SLP:Eu<sup>3+</sup> varied with the doping concentration of Eu<sup>3+</sup>. Figure 5 shows the PLE and PL spectra of the phosphors. A broad band with a peak at 271 nm was referred to the O<sup>2-</sup> → Eu<sup>3+</sup> charge-transfer band (CTB) absorption [28]. The PLE peaks at 362, 383, 394, 363, and 465 nm were attributed to the electron transitions from the <sup>7</sup>F<sub>0</sub> to the <sup>5</sup>D<sub>4</sub>, <sup>5</sup>L<sub>7</sub>, <sup>5</sup>L<sub>6</sub>, <sup>5</sup>D<sub>3</sub>, and <sup>5</sup>D<sub>2</sub> energy levels, respectively. The electron transitions through the <sup>5</sup>D<sub>0</sub> → <sup>7</sup>F<sub>1</sub>, <sup>5</sup>D<sub>0</sub> → <sup>7</sup>F<sub>2</sub>, <sup>5</sup>D<sub>0</sub> → <sup>7</sup>F<sub>3</sub>, and <sup>5</sup>D<sub>0</sub> → <sup>7</sup>F<sub>4</sub> exhibited red to NIR luminescence with peak wavelengths at 593, 615, 656, and 705 nm, respectively. The PL intensity was enhanced by the increase of Eu<sup>3+</sup> doping concentration, as shown in Figure 6. The maximum PL intensity was obtained when a 7 mol% Eu<sup>3+</sup> was doped. However, when a higher Eu<sup>3+</sup> concentration of 9 mol% was doped, the PL intensity was decreased because of the effect of concentration quenching. As compared with the SLP:0.01Eu<sup>3+</sup>, the PL intensity of SLP:0.07Eu<sup>3+</sup> was increased by 4.95-fold at wavelength 615 nm and 3.97-fold at 705 nm. High NIR luminescence was obtained. The phosphor with high luminescence in the NIR biowindow has the potential for bio-image and biosensor applications.

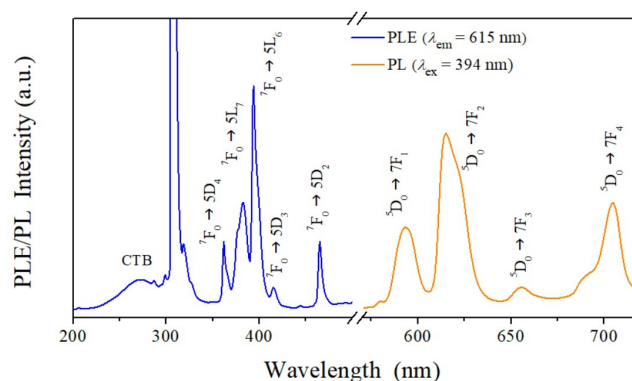


**Figure 5.** PLE and PL spectra of SLP:0.07Eu<sup>3+</sup> phosphor.

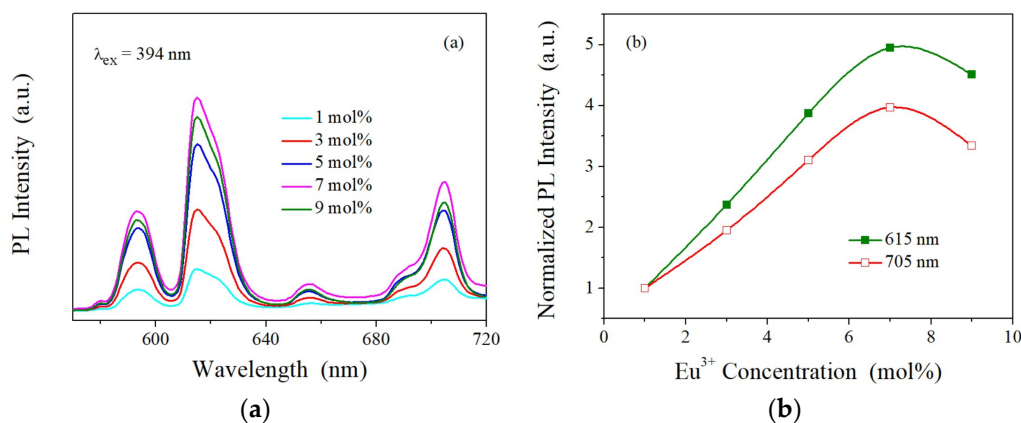


**Figure 6.** (a) PL spectra and (b) normalized PL intensities at wavelengths 615 and 705 nm for SLP:Eu<sup>3+</sup> phosphors synthesized with different Eu<sup>3+</sup> concentrations.

#### 4. Conclusions

The characteristics of red SLP:Eu<sup>3+</sup> phosphors prepared with the coprecipitation method are discussed. The crystallinity and luminescence properties of phosphors altered significantly with the variations of synthesis temperature and doping concentration of Eu<sup>3+</sup>. The maximum PLE and PL intensities were obtained when the phosphor was doped with 7 mol% Eu<sup>3+</sup> and annealed at 1200°C for 2h. The red SLP:Eu<sup>3+</sup> shows high PL intensity both in visible-light and NIR-biowindow regions, with corresponding emission peaks at wavelengths of 615 and 705 nm, respectively. The SLP:Eu<sup>3+</sup> phosphor can be used for bio-image and bio-sensor applications.

**Author Contributions:** conceptualization, S. H. Yang and W. J. Wang; methodology, S. H. Yang and W. J. Wang; validation, S. H. Yang and W. J. Wang; investigation, S. H. Yang and W. J. Wang; resources, S. H. Yang; data curation, S. H. Yang and W. J. Wang; writing—original draft preparation, S. H. Yang and W. J. Wang; writing—review and editing, S. H. Yang; visualization, S. H. Yang. Authorship must be limited to those who have contributed substantially to the work reported.

**Funding:** This research did not receive external funding.

**Acknowledgments:** The authors would like to thank the Ministry of Science and Technology of the Republic of China, Taiwan, for financially supporting this research under contract No. MOST 109-2221-E-992-087.

**Conflicts of Interest:** The authors declare no conflict of interest.

#### References

- Wang, Z.; Lou, S.; Li, P. Single phase tunable warm white-light-emitting Sr<sub>3</sub>La(PO<sub>4</sub>)<sub>3</sub>:Eu<sup>2+</sup>, Sm<sup>3+</sup> phosphor for white LEDs. *Opt. Mater. Express* **2016**, *6*, 114–124. doi:10.1364/OME.6.000114
- Guo, N.; Jia, C.; Li, J.; Zhao, Y.; Ouyang, R.; Lü, W. Color tuning and energy transfer in Eu<sup>2+</sup>/Mn<sup>2+</sup>-doped Ba<sub>3</sub>Y(PO<sub>4</sub>)<sub>3</sub> eulytite-type orthophosphate phosphors. *RSC Adv.* **2015**, *5*, 46517–46524. doi:10.1039/C5RA06347G
- Liu, W.; Wang, X.; Zhu, Q.; Li, X.; Sun, X.; Li, J.-G. Upconversion luminescence and favorable temperature sensing performance of eulytite-type Sr<sub>3</sub>Y(PO<sub>4</sub>)<sub>3</sub>:Yb<sup>3+</sup>/Ln<sup>3+</sup> phosphors (Ln = Ho, Er, Tm). *Sci. Technol. Adv. Mater.* **2019**, *20*, 949–963. doi:10.1080/14686996.2019.1659090
- Fan, B.; Zhao, W.; Han, L. Eu<sup>3+</sup> co-doped Sr<sub>3</sub>Gd(PO<sub>4</sub>)<sub>3</sub>:Dy<sup>3+</sup> phosphors: luminescence properties and color-tunable white-light emission for NUV-WLEDs. *Appl. Phys. A* **2020**, *126*, 1–10. doi:10.1007/s00339-020-3444-5
- Shi, Q.; Huang, Y.; Ivanovskikh, K.V.; Pustovarov, V.A. Luminescence properties and host sensitization study of Ba<sub>3</sub>La(PO<sub>4</sub>)<sub>3</sub>:Ce<sup>3+</sup> with (V)UV and X-ray excitation. *J. Alloys Compd.* **2020**, *817*, 152704. doi:10.1016/j.jallcom.2019.152704
- Wang, Q.; Huo, J.; Zheng, Y.; Pang, S.; He, Z. Design of red/green emissive lanthanide activated nano-materials by supersonic and microwave co-irradiations. *Opt. Mater.* **2013**, *35*, 1146–1150. doi:10.1016/j.optmat.2012.12.026
- Zheng, X.; Kankala, R.K.; Liu, C.-G.; Wang, S.-B.; Chen, A.-Z.; Zhang, Y. Lanthanides-doped near-infrared active upconversion nanocrystals: Upconversion mechanisms and synthesis. *Coord. Chem. Rev.* **2021**, *438*, 213870. doi:10.1016/j.ccr.2021.213870
- Thoř, T.; Rubeřova, K.; Jakeř, V.; Cajzl, J.; Nadherny, L.; Mikolasova, D.; Kučerkova, R. Lanthanide-doped Lu<sub>2</sub>O<sub>3</sub> phosphors and scintillators with green-to-red emission. *J. Lumin.* **2019**, *215*, 116647. doi:10.1016/j.jlumin.2019.116647
- Shui, X.; Zou, C.; Zhang, W.; Bao, C.; Huang, Y. Effect of M<sup>3+</sup> (M = Bi, Al) co-doping on the luminescence enhancement of Ca<sub>2</sub>ZnSi<sub>2</sub>O<sub>7</sub>:Sm<sup>3+</sup> orange-red-emitting phosphors. *Ceram. Int.* **2021**, *47*, 8228–8235. doi:10.1016/j.ceramint.2020.11.182
- Li, Y.; Jiang, J.; Lv, Q.; Shao, B.; Wang, C.; Zhu, G. Structural and spectroscopic features of high color purity red-emitting phosphors Sr<sub>19</sub>Mg<sub>2</sub>(PO<sub>4</sub>)<sub>14</sub>:Re<sup>3+</sup> (Re<sup>3+</sup> = Eu<sup>3+</sup>, Sm<sup>3+</sup>, Pr<sup>3+</sup>). *Spectrochim. Acta, Part A* **2021**, *251*, 119417. doi:10.1016/j.saa.2020.119417
- Lei, Z.; Zhang, W.; Li, B.; Guan, G.; Huang, X.; Peng, X.; Zou, R.; Hu, J. A full-spectrum-absorption from nickel sulphide nanoparticles for efficient NIR-II window photothermal therapy. *Nanoscale* **2019**, *11*, 20161–20170. doi:10.1039/c9nr04005f
- Sun, D.; Zhang, L.; Hao, Z.; Hao, Z.; Wu, H.; Wu, H.; Luo, Y.; Yang, L.; Liu, F.; Zhang, J. Multi-peaked broad-band red phosphor Y<sub>3</sub>Si<sub>6</sub>N<sub>11</sub>:Pr<sup>3+</sup> for white LEDs and temperature sensing. *Dalton Trans.* **2020**, *49*, 17779–17785. doi:10.1039/d0dt03532g
- Yan, G.; Zhang, W.; Huang, Y.; Zhang, P.; Li, J. Luminescence enhancement for Y<sub>2</sub>Mo<sub>4</sub>O<sub>15</sub>:Pr<sup>3+</sup> red-emitting phosphors by Tb<sup>3+</sup> co-doping. *J. Mater. Sci.: Mater. Electron.* **2019**, *30*, 14589–14599. doi:10.1007/s10854-019-01831-x
- Wu, L.; Bai, Y.; Wu, L.; Yi, H.; Kong, Y.; Zhang, Y.; Xu, J. Sm<sup>3+</sup> and Eu<sup>3+</sup> codoped SrBi<sub>2</sub>B<sub>2</sub>O<sub>7</sub>: a red-emitting phosphor with improved thermal stability. *RSC Adv.* **2017**, *7*, 1146–1153. doi:10.1039/c6ra26752a
- We, C.; Xu, D.; Yang, Z.; Li, J.; Chen, X.; Li, X.; Sun, J. A novel orange-red emitting phosphor Sr<sub>2</sub>LuTaO<sub>6</sub>:Sm<sup>3+</sup> for WLEDs. *J. Mater. Sci.: Mater. Electron.* **2019**, *30*, 9303–9310. doi:10.1007/s10854-019-01260-w
- Bednarova, Z.; Kalina, J.; Hajek, O.; Sanka, M.; Komprdova, K. Spatial distribution and risk assessment of metals in agricultural soils. *Geoderma* **2016**, *284*, 113–121. doi:10.1016/j.geoderma.2016.08.021
- Lei, Z.; Zhang, W.; Li, B.; Guan, G.; Huang, X. A full-spectrum-absorption from nickel sulphide nanoparticles for efficient NIR-II window

- photothermal therapy. *Nanoscale* **2019**, *11*, 20161–20170. doi:10.1039/c9nr04005f
18. Yang, H.; Zhao, W.; Lin, X.; Liao, Z.; Nie, Z.; Luo, L.; Zhang, W.; Hu, Z.; Zhong, J. Hundreds of times of photo-stimulation with low energy light as a new reused bio-imaging phosphor from Cr<sup>3+</sup>, Si<sup>4+</sup>-doped Y<sub>3</sub>Ga<sub>5</sub>O<sub>12</sub>. *J. Lumin.* **2020**, *219*, 116871. doi:10.1016/j.jlumin.2019.116871
  19. Taktak, O.; Souha, H.; Kammoun, S. Optical properties of the phosphors Zn<sub>2</sub>SnO<sub>4</sub>:Cr<sup>3+</sup> with near-infrared long-persistence phosphorescence for bio-imaging applications. *J. Lumin.* **2020**, *228*, 117563. doi:10.1016/j.jlumin.2020.117563
  20. Lyu, T.; Dorenbos, P. Designing thermally stimulated 1.06 μm Nd<sup>3+</sup> emission for the second bioimaging window demonstrated by energy transfer from Bi<sup>3+</sup> in La-, Gd-, Y-, and LuPO<sub>4</sub>. *Chem. Eng. J.* **2019**, *372*, 978–991. doi:10.1016/j.cej.2019.04.125
  21. Yang, J.; Zhao, Y.; Meng, Y.; Zhu, H.; Yan, D.; Liu, C.; Xu, C.; Zhang, H.; Xu, L.; Li, Y.; Liu, Y. Irradiation-free photodynamic therapy *in vivo* induced by enhanced deep red afterglow within NIR-I bio-window. *Chem. Eng. J.* **2020**, *387*, 124067. doi:10.1016/j.cej.2020.124067
  22. Xu, W.; Zhao, D.; Zheng, L.; Zhang, Z.; Cao, W. NIR to NIR luminescence thermometry in core/multishells-structured nanoparticles operating in the biological window. *J. Lumin.* **2020**, *225*, 117358. doi:10.1016/j.jlumin.2020.117358
  23. Rivera-Enríquez, C.E.; Fernández-Osorio, A.L. Synthesis of YVO<sub>4</sub>:Eu<sup>3+</sup> nanophosphors by the chemical coprecipitation method at room temperature. *J. Lumin.* **2021**, *236*, 118110.
  24. Kee, C.C.; Ang, B.C.; Metselaar, H.S.C. Synthesis of europium-doped calcium silicate hydrate via hydrothermal and coprecipitation method. *Ceram. Int.* **2021**, *47*, 4803–4812. doi:10.1016/j.ceramint.2020.10.050
  25. Smara, Z.; Cheroura, Y.; Boyer, D.; Potdevin, A.; Chafa, A.; Ziane, O.; Mahiou, R. Energy transfer and luminescent properties of Eu<sup>3+</sup>, Tb<sup>3+</sup>, Eu<sup>3+</sup>-Yb<sup>3+</sup> and Tb<sup>3+</sup>-Yb<sup>3+</sup> doped α-NaYF<sub>4</sub> nanophosphors prepared by coprecipitation route. *Opt. Mater.* **2020**, *104*, 109932. doi:10.1016/j.optmat.2020.109932
  26. Yang, S.-H.; Wang, W.-W.; Lee, Y.-C.; Chiang, P.-J. Luminescence enhancement of spherical Sr<sub>3</sub>La(PO<sub>4</sub>)<sub>3</sub>:Eu<sup>3+</sup> red nanophosphor with core-shell configuration and added sensitizer for low-voltage field-emission lamp. *J. Alloys Compd.* **2019**, *783*, 785–792. doi:10.1016/j.jallcom.2018.12.270
  27. Stypczyńska, A.; Nixon, T.; Mason, N. X-ray radiation of poly-L-arginine hydrochloride and multilayered DNA-coatings. *Eur. Phys. J. D* **2014**, *68*, 1–10. doi:10.1140/epjd/e2014-40845-8

**Publisher's Note:** IIKII stays neutral with regard to jurisdictional claims in published maps and institutional affiliations.

**Copyright:** © 2021 The Author(s). Published with license by IIKII, Singapore. This is an Open Access article distributed under the terms of the [Creative Commons Attribution License](https://creativecommons.org/licenses/by/4.0/) (CC BY), which permits unrestricted use, distribution, and reproduction in any medium, provided the original author and source are credited.